Since January 2020 Elsevier has created a COVID-19 resource centre with free information in English and Mandarin on the novel coronavirus COVID-19. The COVID-19 resource centre is hosted on Elsevier Connect, the company's public news and information website.

Computational Toxicology 24 (2022) 100247

Contents lists available at ScienceDirect

Computational Toxicology

journal homepage: www.sciencedirect.com/journal/computational-toxicology

Potential inhibitory activity of phytoconstituents against black fungus: *In silico* ADMET, molecular docking and MD simulation studies

Narmin Hamaamin Hussen [a], Aso Hameed Hasan [b,c], Joazaizulfazli Jamalis [c], Sonam Shakya [d], Subhash Chander [e], Harsha Kharkwal [e], Sankaranaryanan Murugesan [f], Virupaksha Ajit Bastikar [g], Pramodkumar Pyarelal Gupta [h,*]

[a] Department of Pharmacognosy and Pharmaceutical Chemistry, College of Pharmacy, University of Sulaimani, Sulaimani 46001, Iraq
[b] Department of Chemistry, College of Science, University of Garmian, Kalar 46021, Kurdistan Region, Iraq
[c] Department of Chemistry, Faculty of Science, Universiti Teknologi Malaysia, 81310 Johor Bahru, Johor, Malaysia
[d] Department of Chemistry, Faculty of Science, Aligarh Muslim University, Aligarh 202002, India
[e] Amity Institute of Phytochemistry and Phytomedicine, Amity Univ Uttar Pradesh, Noida 201313, India
[f] Medicinal Chemistry Research Laboratory, Department of Pharmacy, Birla Institute of Technology and Science Pialni, Pilani Campus, Pilani 333031, Rajasthan, India
[g] Amity Institute of Biotechnology, Amity University Maharashtra, Mumbai-Pune Expressway, India
[h] School of Biotechnology and Bioinformatics, D Y Patil Deemed to be University, Navi Mumbai, Maharashtra, India

ARTICLE INFO

Edited by Dr. Mark Cronin

Keywords:
COVID-19
Black fungus
Rhizopus oryzae
Molecular docking
Molecular dynamics
ADMET prediction

ABSTRACT

Mucormycosis or "black fungus" has been currently observed in India, as a secondary infection in COVID-19 infected patients in the post-COVID-stage. Fungus is an uncommon opportunistic infection that affects people who have a weak immune system. In this study, 158 antifungal phytochemicals were screened using molecular docking against glucoamylase enzyme of Rhizopus oryzae to identify potential inhibitors. The docking scores of the selected phytochemicals were compared with Isomaltotriose as a positive control. Most of the compounds showed lower binding energy values than Isomaltotriose (-6.4 kcal/mol). Computational studies also revealed the strongest binding affinity of the screened phytochemicals was Dioscin (-9.4 kcal/mol). Furthermore, the binding interactions of the top ten potential phytochemicals were elucidated and further analyzed. *In-silico* ADME and toxicity prediction were also evaluated using SwissADME and admetSAR online servers. Compounds Piscisoflavone C, 8-O-methylaverufin and Punicalagin exhibited positive results with the Lipinski filter and drug-likeness and showed mild to moderate of toxicity. Molecular dynamics (MD) simulation (at 300 K for 100 ns) was also employed to the docked ligand-target complex to explore the stability of ligand-target complex, improve docking results, and analyze the molecular mechanisms of protein-target interactions.

1. Introduction

Mucormycosis, is known as black fungus is an uncommon and deadly fungal infection, that was previously termed as 'zygomycosis' [1]. Mucormycosis is caused by fungi belonging to the Mucorales order and the family *Mucoraceae*, first reported in the history by Paultauf [2,3]. Rhizopus oryzae is the primary fungus responsible for around 70 % of all disease manifestation and 90 % of all rhinocerebral cases [4]. Generally, mucormycosis has emerged in immunocompromised patients, including uncontrolled diabetes, bone marrow transplantation, other types of metabolic acidosis, corticosteroid therapy, and solid organ, malignant haematological disorders and deferoxamine therapy in patients receiving haemodialysis [5,6]. Recently, the pandemic coronavirus disease-2019 (COVID-19) which is caused by SARS-CoV 2 is another fiery example of a patient's immune system weakening whereby the patient becomes susceptible to such opportunistic fungal infections. There is no genetic link between COVID and mucormycosis, they are immunologically interconnected [7–13]. COVID-19 infection increases the level of pro-inflammatory cytokines like IL-1, IL-6, tumor necrosis factor alpha (TNF-α), and may decrease the number of immune cells that maintaining the immune system homeostasis such as CD4 + and CD8 + T cells, which may lead to increased susceptibility for those patients with bacterial and fungal co-infections [14].

Just after the COVID-19 s wave, significantly high number of black

* Corresponding author.
E-mail address: pramodkumar785@gmail.com (P. Pyarelal Gupta).

https://doi.org/10.1016/j.comtox.2022.100247
Received 7 July 2022; Received in revised form 17 September 2022; Accepted 20 September 2022
Available online 24 September 2022

fungus cases were reported in India as post-COVID infections [15–17]. Incidences were found to be relatively high in the patients who received corticosteroid including patients admitted to intensive care units and longer duration of hospital stay. Corticosteroid was extensively used during COVID-19 in order to reduce inflammation in lungs and repairing damages caused by the overdriving of immune system of the body. Steroid therapy weakens the immune system of the host and both diabetic and non-diabetic patients lead to a rise in blood sugar levels which both factors increase the susceptibility of host toward mucormycosis. Moreover, diabetic condition is counted as a high-risk factor for black fungal infection [18–21]. Therefore, if this condition of mucormycosis without any protection, it can readily enter the body and cause severe infection, leading the patient to inevitable death. The route of entry by this fungus is *via* inhalation of the spore, so it is advisable to keep the house mold-free [22,23]. The aggressive form of coronavirus infects the lungs, which makes the patients more prone to get infections that are airborne, including mucormycosis [24].

Black fungus affects multiple organs, predominantly, brain, lungs and sinuses, and it has symptoms are similar to COVID-19 infections including fever, cough, etc., which both diseases can be distinguished by the clinical investigations. Other symptoms that are linked to black fungus infections are as follows: swelling in one side of the face, headache, fever, nasal congestion, black lesions on the nose or inside the mouth [7,25–27]. Most common treatment strategies involve high doses of liposomal amphotericin B, and sometimes surgical resections whenever required. The mortality rate for mucormycosis is higher than 50 % and depends on the affiliated diseases [5,22,28,29]. The study was done in India by Patel A. *et al.*, whereby diabetes was a risk factor, with or without ketoacidosis occurring in 73.5 % of patients with mucormycosis [30].The death rate is 90–100 % in patients with disseminated disease, central nervous system infection or prolonged neutropenia [31–35]. Unfortunately, the unacceptably high mortality rate, limited options for therapy, the high cost of managing mucormycosis, and the highly disfiguring surgical therapy, etc., drive the urgent need of newer therapeutic drugs to treat the disease [6].

Discovery and development by de nava design is a time-consuming and costly process, so, repurposing can be an appropriate strategy to search potent molecules from the pre-existing databases. The computational approaches such as molecular docking and dynamics simulations, *in silico* ADMET and drug-likeness predictions are mostly used to discovery and development of drug candidates from several databases. Considering literature data, many active agents against fungal infections have been documented in the herbal medicine. The natural products comprising of a diverse range of secondary metabolites including flavonoids, coumarins, limonoids, terpenoids, phenolic compounds, tannins, quinones, saponins, xanthones, alkaloids, peptides, and biosurfactants were reported having *in vitro* antifungal properties [36–45]. Therefore, in recent year research on these phytochemicals and their derived compounds have been the subject of increased investigation due to their importance in drug design. Plants have a variety of active compounds having antifungal activity against various fungus strains, these are important to humans. For instance, there are currently-two major drug classes in use (amphotericin B, the gold standard and armamentarium and the lipopeptide caspofungin) are the important antifungal drugs, which are derived from natural products [46–49].

In this work, 158 phytochemicals contain of terpenoids, limonoids, phenolic compounds, tannins, flavonoids, coumarins, quinones, saponins, xanthones, alkaloids, peptides and other classes of compounds were screened based on their reported bioactivity to discovery of hit for therapeutic against protein of mucormycosis. In this study, we selected the glucoamylase enzyme of Rhizopus oryzae (RoGA) for screening of phytochemical. Glucoamylase (EC 3.2.1.3), also known as amyloglucosidase; glucan 1,4-α-glucosidase; amylase; 1,4-α-D-glucanglucohydrolase is amylolytic enzyme, that yieldsβ-D-glucose from the starch and polysaccharide by hydrolyzing α-1,4 and α-1,6 linkages, produced by the different sources such as fungi (Aspergillus, Penicillium spp. Rhizopus oryzae), yeast and bacteria [50,51]. Glucoamylase (GA) belongs to the family of the glycoside hydrolase 15 (GH15) due to its structural similarity to that enzyme group or family. Glycoside hydrolase family 15 comprises enzymes with several known activities; glucoamylase; alpha-glucosidase; glucodextranase [52]. RoGA is comprising of starch binding domain at *N*-terminal and catalytic domain at C-terminal terminal, connected by an *o*-glycosylated linker. It can hydrolyze both amylose and amylopectin by breaking α-1,4 as well as α-1,6 glycosidic bonds and produce glucose units [53].

Glucose is an essential nutrient for the growth of fungal infections because these metabolites serve as carbon skeletons for the biosynthesis of other molecules as well as serving precursors for energy production and being involved in cellular signaling pathways in fungi [54]. GA among these, Rhizopus spp is well known for significant production of glucoamylase enzyme, which plays an important role in fungal growth and life cycle [55]. Glucoamylase is also produced within the human intestinal body as an essential enzyme besides carbohydrates and long-chain starches are broken down into sugars by this enzyme, which the body uses as fuel. The primary function of all essential enzymes is to break down most starches and carbohydrates to their purest forms so that the body can obtain nutrients from these foods [56].

Several studies have been reported that Glucoamylase inhibitors exhibited antimicrobial, antifungal, antibacterial activities and anti-diabetic for type II diabetes [57–59]. There are many studies have been revealed that Rhizopus oryzae would use its spore coat protein CotH3 of Mucorales to interact with glucose-regulated protein 78 (GRP78) as a receptor on nasal epithelial cells to penetrate and destroy the cells. The ketone body levels (hallmark features of Diabetic ketoacidosis (DKA)), iron, and high glucose, increase expression of the CotH3 and GRP78 proteins, potentially leading to frequently fatal cerebral mucormycosis and rhinoorbital [60–62].Increasing expression of the GRP78 receptor in COVID-19 patients may promote Mucorales spore binding, resulting in increased endothelial invasion and damage [63]. Teclegiorgis *et al.*, found that inhibiting Rhizopus CotH3 expression blocked invasion even in mammalian cells overexpressing GRP78, showing the importance of this fungus protein in pathogenicity. It was also found that the Polyclonal antibodies produced toward both peptides in CotH3′s GRP78-binding domain inhibited fungal invasion and adhesion of endothelial cells *in vitro* and protected DKA mice from Rhizopus oryzae associated pulmonary mucormycosis [62]. Likewise, repression of GRP78 and CotH3 expression by GA inhibitors is probably due to their ability to block glucose production, which would protect endothelial cells from Rhizopus oryzae -induced endocytosis and subsequent damage.

2. Experimental

2.1. Ligand preparation

A list of 158 bioactive compounds was collected from various herbals that were reported as anti-fungal agents [64–113]. The 3D structure of phytochemicals were downloaded from Pubchem database (https://pubchem.ncbi.nlm.nih.gov/) in SDF format. The structures that were not available in PubChem were drawn using the Avogadro tool (version 1.2.0) (https://avogadro.cc/) [114]. The structures were further converted into PDBQT format using Open Babel software (version 2.3.1) (https://openbabel.org/wiki/Main_Page) [115]. MMFF94 force field and conjugate gradient optimization algorithm were used to minimize the ligand energy in 200 steps using PyRx-Python prescription 0.8 [116].

2.2. Receptor preparation

The 3D crystal structure of Glucoamylase enzyme(PDB ID: 4BFO) was retrieved from RCSB protein data bank (https://www.rcsb.org/structure/4BFO) [117]. The resolution of the obtained structures

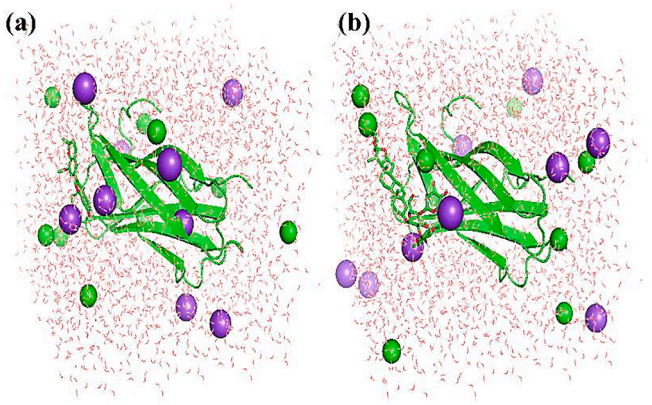

Fig. 1. Protein-ligand complex(a) Dioscin and (b) Piscisoflavone C in triclinic box solvated with water molecules and neutralized with 9 Na^+ and 9 Cl^- ions (0.15 M salt).

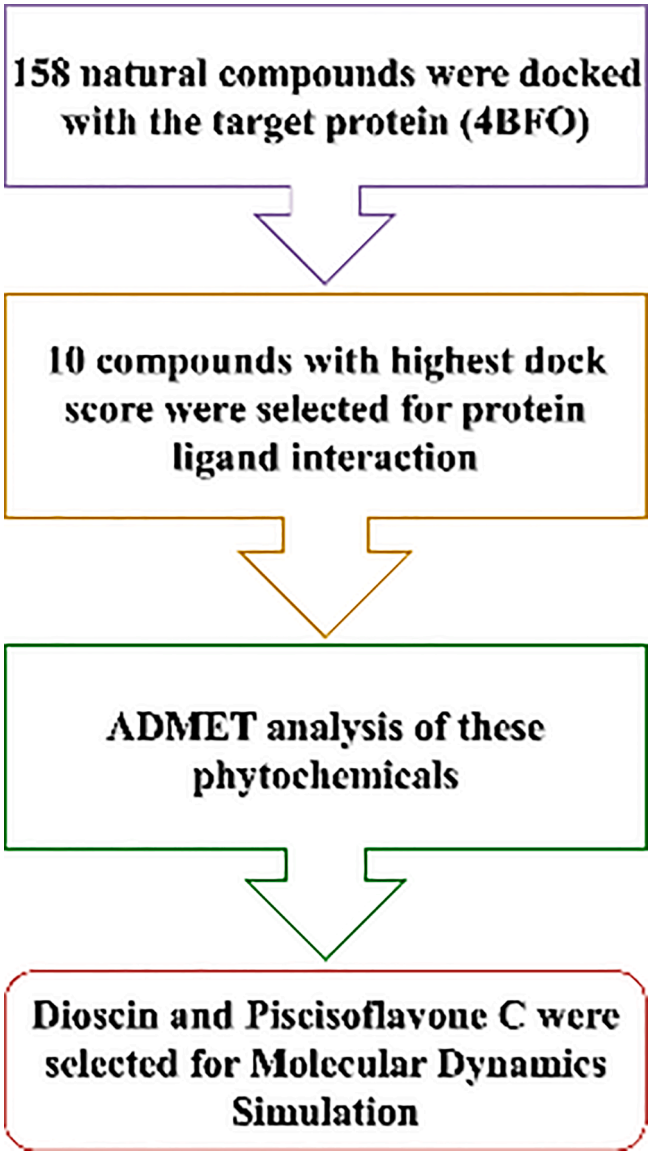

Fig. 2. The molecular structure of the best 10 screened phytochemicals.

was 1.18 Å. The file was opened using BIOVIA Discovery Studio Visualizer (v17.2.0.16349). The protein preparation was carried out by eliminating the native inhibitor and other heteroatoms, including water molecules. The receptor was then saved as pdb format. AutoDock Tool [118] was used to add polar hydrogen atoms to the receptor, to determine Kollman charges, and Partial charges were assigned. Then, the prepared file was saved as pdbqt format.

2.3. Molecular docking

The original ligand was re-docked on the target receptor to validate the docking method, BIOVIA Discovery Studio Visualizer (DSV) was used to eliminate this ligand from the receptor. The grid box parametric dimension values were adjusted as X = -21.75700, Y = -0.386824 and Z = 11.718029. The exhaustiveness value was set as 8 to obtain an efficient binding conformation pose of the protein–ligand complex. Afterward, the retrieved phytochemicals were docked against the protein of target with PDB ID:4BFO. AutoDock Vina [119]. was used to perform the docking simulation. Finally, AutoDock Vina generated a docked complex for each ligand with various conformation and affinity scores (in kcal/mol) and ranked them based on the lowest binding energy theory (kcal/mol) of docked complexes (whereby more negative value means greater binding affinity). The best protein–ligand complex docked pose were analyzed and graphically visualized by DSV (https://www.3ds.com/products-services/biovia/).

2.4. In-silico predicted ADMET profiles

In-silico prediction of ADME properties of the selected phytochemicals was carried out using SwissADME online server [120], while toxicity was predicted using the Organ toxicity and Genomic toxicity model from admetSAR 2.0 [121] as reported in literature [122]. The organ toxicity is classified under the category: Drug-induced liver injury, Human ether-a-go-go-related gene (hERG) inhibition, acute toxicity, Eye injury and Eye corrosion. The genomic toxicity is classified: ames mutagenesis, carcinogenesis and micronucleus assay. The smile notation for all the selected 10 compounds was considered as the starting point and input to the SwissADME and admetSAR 2.0 webserver and thereby ADME and toxicity predictions were carried out.

2.5. Molecular dynamics (MD) simulations

The best docked poses of Dioscin and Piscisoflavone C obtained from the docking was used further for MD simulation and evaluating their conformational space and inhibitory potential. The GROMACS package (Ver. 2019.2) with GROMOS96 43a1 force field was carried out to analysis the MD simulation. Parameter files and topology of ligands were prepared utilizing the latest CGenFF *via* CHARMM-GUI [123,124]. The SPC water models that extended 10 from the protein was used to solvate the structures of both complexes in a triclinic box [125]. In order to mimic physiological salt concentration, 9 Na^+ and 9 Cl^- ions (0.15 M salt) were added to neutralize the systems for both cases, as shown in Fig. 1. In the NPT/NVT equilibration run, both systems were introduced to periodic boundary conditions (1.0 bar, 300 K) utilizing a Leap-frog MD integrator for a 100 ns [126]. For electrostatic interactions, the particle-mesh Ewald protocol was applied [127]. The force-based switching algorithm was applied to truncate interactions (non-bonded) above 10 and 12 Å [128]. Minimization of energy was used to eliminate bad contact inside the system *via* the steepest descent with 5000 steps. Additionally, to avoid the cold solute-hot solvent problem, the indexing system applied temperature coupling into both water and non-water components. Furthermore, for NVT/NPT equilibrations run, a modified Berendsen thermostat and a Parrinello-Rahmanbarostat were performed. Trajectory analysis was carried out using GROMACS analysis. Calculation of the root mean square deviation (RMSD) and root mean square fluctuations (RMSF) of receptor were carried out utilizing gmxrms and gmx rmsf, respectively. The gmx sasa and gmx gyrate tools

Table 1
The docking score of the best 10 screened phytochemicals and their interactions with the enzyme.

Entry	Compounds	B.E (kcal/mol)	Interactions		
			H-Bond	Hydrophobic	Others
1	Hopeanolin	**−8.8**	Tyr32, Lys34, Phe58	π-π stacked: Tyr32, Phe58; π-alkyl:Phe58	Glu68 (π-anion)
8	Vaticanol E	**−8.7**	Lys34, Lys35, Ser57	π-alkyl:Phe58	
11	Vaticanol B	**−8.5**	Tyr32, Lys34, Ser57, Phe58	π-π stacked: Tyr32, Phe58, Trp70; π-alkyl: Tyr32, Phe58	Glu68 (π-anion)
12	alpha-Viniferin	**−8.6**	Asn29, Tyr32, Tyr67, Glu68	π-π stacked: Tyr32, Phe58; alkyl: Phe58, Pro61	Glu68 (π-anion)
13	Pauciflorol A	**−8.7**	Asn29, Tyr32, Ser65	π-π stacked: Tyr32, Phe58; π-alkyl: Tyr32, Phe58	Glu68 (π-anion)
31	Dioscin	**−9.4**	Lys34, Lys35, Ala56, Ser57, Phe58	π-alkyl: Tyr32, Phe58	Phe58 (π-sigma)
114	8-O-methylaverufin	**−8.3**	Lys34, Lys35, Phe58	π-alkyl: Tyr32, Phe58, Trp70	Ala55 (π-sigma)
118	Piscisoflavone C	**−8.3**	Asn29, Lys34	π-π stacked: Tyr32, Phe58; alkyl:Pro61	Glu68 (π-anion)
139	Punicalin	**−8.3**	Tyr32, Lys34, Lys35, Ala56, Ser57, Phe58		
145	Punicalagin	**−8.2**	Lys34, Lys35, Ser57	π-π stacked: Tyr32, Phe58; π-alkyl: Ala55	
	Isomaltotriose	**−6.4**	Tyr32, Lys34, Ser57, Phe5		Tyr32 (π-sigma)

B.E: Binding Energy.

were used to calculate the solvent accessible surface area (SASA) and radius of gyration (RG), respectively. Hydrogen bonds were analyzed by gmxh bond tool. Grace Software was utilized to generate the plots. The complex structure was visualized by PyMol and VMD [129,130]. The simulation time for the ligand-receptor was 10.4 and 10.3 h for Dioscin and Piscisoflavone C, respectively, for 100 ns.

3. Results

3.1. Molecular docking

Selected 158 anti-fungal phytochemicals were docked against target enzyme. The native ligand, Isomaltotriose was used as the control for comparative purpose. Molecular docking of these phytochemicals revealed binding affinity ranging from −4.1 to −9.4 kcal/mol. Among the 158 phytochemicals screened, 123 phytochemicals showed docking energy values higher than Isomaltotriose (-6.4 kcal/mol). The interactions of the best 10 compounds (Fig. 2) is depicted in Table 1. These compounds that have higher potential making hydrogen bond and hydrophobic interactions with Tyr32, Lys34, Lys35, Phe58 and Ser57 were common interacting residues.

3.2. In silico predicted ADMET profiles

3.2.1. Predicted ADME profiles

The physico-chemical properties of the top ten compounds were given in the Table 2.

3.2.2. Predicted toxicity results

The organ toxicity and genome toxicity were summarized in Table 3.

3.3. Molecular dynamics simulation

The best docked conformations of each Dioscin and Piscisoflavone C, which exhibited significant results based on *in-silico* predicted ADMET analysis, were selected for 100 ns MD simulation. The best conformation was utilizing to set up dynamics simulation process in a high-throughput manner for analyzing the mechanism of ligands binding dynamics with target receptor under clearly expressed water conditions.

4. Discussion

Molecular docking studies investigating for mucormycosis inhibitors exhibited that the natural compounds are already reported for inhibiting the growth of *Rhizopus oryzae*. The fungal cell walls and enzymes have been previously founding as an attractive target for the discovery of new antifungal agents. According to the results obtained, it has been shown that the higher dock score was against the receptor of *Rhizopus oryzae*, and even comparatively higher than the native ligand, Isomaltotriose. Evidence from several in *vivo*, *in vitro*, and animal studies suggests that phenolic compounds such as phenols, coumarins, flavonoids, tannins, quinines, xanthones and stilbenoids from natural sources have antifungal properties and, it's also shown that their activity is mainly due to the site (s) and the number of hydroxyl groups in a compound are assumed to be related to their relative toxicity to microorganisms. As previously stated, increasing toxicity is related to more hydroxylation

Table 2
Results of predicted ADME properties of the 10 best compounds.

Entry	Formula	M.W	FC	HBA	HBD	MR	TPSA	X3	WS	GI.A	B.P	Pg	LV	B.S	S.A
1	$C_{42}H_{28}O_{10}$	692.67	0.14	10	5	186	162.98	4.9	P.S	Low	No	Yes	1	0.11	7.05
8	$C_{42}H_{32}O_9$	680.7	0.14	9	8	189.88	171.07	6.84	P.S	Low	No	Yes	2	0.17	6.24
11	$C_{56}H_{42}O_{12}$	906.93	0.14	12	10	252.25	220.76	9.12	Ins	Low	No	Yes	3	0.17	7.55
12	$C_{42}H_{30}O_9$	678.68	0.14	9	6	187.09	149.07	6.83	P.S	Low	No	Yes	2	0.17	6.41
13	$C_{42}H_{32}O_9$	680.7	0.14	9	8	189.88	171.07	6.84	P.S	Low	No	Yes	2	0.17	6.24
31	$C_{45}H_{72}O_{16}$	869.04	0.96	16	8	216.42	235.68	1.34	M.S	Low	No	Yes	3	0.17	10
114	$C_{21}H_{18}O_7$	382.36	0.33	7	2	97.87	102.29	3.3	M.S	High	No	Yes	0	0.55	4.85
118	$C_{21}H_{18}O_5$	350.36	0.19	5	1	100.56	68.9	3.72	M.S	High	Yes	No	0	0.55	3.83
139	$C_{34}H_{22}O_{22}$	782.53	0.18	22	13	180.45	385.24	−0.29	M.S	Low	No	Yes	3	0.17	6.74
145	$C_{20}H_{16}O_5$	336.34	0.15	5	2	96.09	79.9	3.94	M.S	High	No	No	0	0.55	3.76

M.W: Molecular weight (g/mol), FC: Fraction Csp^3, HBA: Number of H-bond acceptors, HBD: Number of H-bond donors, MR: Molar Refractivity, TPSA: Topological polar surface area (Å^2), X3: XLOGP3,WS: Water Solubility Class, GI.A: Gastrointestinal Absorption, B.P: Blood Brain-Barrier permeant, Pg: P-glycoprotein substrate, LV: Lipinski Violation, B.S: Bioavailability Score, S.A: Synthetic accessibility.

Table 3
Results of predicted toxicity of the 10 best compounds.

Entry	1	8	11	12	13	31	114	118	139	145
Organ Toxicity										
Acute Oral Toxicity	II	III	III	III	III	III	III	III	III	III
Eye corrosion	–	–	–	–	–	–	–	–	–	–
Eye irritation	–	–	–	–	–	–	–	+	–	+
Hepatotoxicity	+	+	+	+	+	–	+	+	+	+
Human either-a-go-go inhibition	+	+	+	+	+	+	–	–	+	–
Genomic toxicity										
Ames mutagenesis	+	–	–	–	–	–	+	–	+	–
Carcinogenicity (trinary)	Danger	N.R	N.R	Warning	N.R	N.R	N.R	Danger	N.R	N.R
micronuclear	+	+	+	+	+	–	–	+	+	+

N.R: Non-required.

[80,108,113]. Moreover, phenol compounds with higher degree of oxidation were shown more inhibitory activities [131]. Studies also indicated that the antifungal activities of flavonoids like isopiscerythrone, allolicoisoflavone A, piscisoflavones A, B and C, licoflavone A, papyriflavonol A, quercetin, hesperidin, neohesperidin and naringin, because of their ability to bind to extracellular and soluble proteins, as well as to bind to fungal cell walls. The more lipophilic nature of flavonoids may also account for the disrupted fungal membranes [69,80,90,96,99,107]. A large number of studies have established that terpenoids such as estragole, encelin and panicutine exhibit antifungal activity. Terpenes' mechanism of action is not fully explained, but it is thought to include membrane disruption due to their lipophilic nature. The addition of a methyl group to the hydrophilicity of kaurene diterpenoids drastically decreased their antimicrobial activity as reported by Mendoza *et al.*, [132]. Encelin, a known sesquiterpene lactone extracted from the Mexican species Montanoa speciosa, has a significant effect on fungal cell development and morphogenetic processes [133]. Limonoids are highly oxygenated and modified triterpenes and to date, more than 300 limonoids are isolated, which include: obacunone, corosolic acid, maslinic acid, hydroxyseneganolide, oleanane, epoxyazadiradione,7-deacetylgedunin, oleanolic acid, ursolic acid, limoninglucoside, azadiradionolide, eugenol,1,3-dideacetyl-7-deacetoxy-7-oxokhivorin, seneganolide A, B., methyl 6-hydroxyangolensate and gedunin. Limonin is the first isolated limonoids found in medicinal plants, such as citrus, neem, tulsi and licorice. Limonoids have been identified as having various biological properties including antibacterial, antifungal, antiviral, antimalarial, and anticancer [72,78,80,106]. Saponins are steroidal or terpenoid-based glycosides with surface-active properties such as saponin and sapindoside B. CAY-1, a triterpene saponin from the *Capsicum* frutescens, was reported to be potent against 16 different fungal strains, including *C. neoformans*, *A. fumigatus*, and *Candida spp*. It has been shown that the antifungal properties of CAY-1 can be attributed to the breakdown of fungal cell membrane integrity [91,134,135]. Nowadays, an alkaloid namely, 2-(3,4-dimethyl-2,5-dihydro-1*H*-pyrrol-2-yl)-1-methylethyl pentanoate was extracted from the *Daturametel* and displayed in vivo and *in vitro* activities against both species (*Candida* and *Aspergillus)*. The antifungal alkaloids such as β-carboline, derived alkaloids including two phenylethylamine along with tryptamine, and *N*-methyl-*N*-formyl-4-hydroxy-beta-phenylethylamine from *Cyathobasis fruticulosa*, haloxylines A and B, new piperidine from *Haloxylon salicornium* all displayed antifungal potentials. The reduced fungal growth of *Aspergillus flavus* has been shown to correlate with reduced aflatoxin production in laboratory studies [136]. Jatrorrhizine isolated from *Mahonia aquifolium* was the most potent towards all fungal species [68,80]. Fig. 3 shows the experimental part of this research.

The docking studies revealed that the Dioscin binds to the target enzyme with highest dock score of −9.4 kcal/mol. The illustration of molecular docking for the interactions of Dioscin and receptor was depicted in Fig. 4a, b. The analysis of the best docked pose of Dioscin exhibited that the amino acid residues including Lys34, Lys35, Ala56 and Ser57 had formed hydrogen bond interactions. Additionally, Phe58 established two interactions including hydrogen bond, π-alkyl and π-sigma. Moreover, Dioscin interacted with residue Tyr32 *via* π-alkyl interaction. The Piscisoflavone C which exhibited significant *in silico* ADMET profile was selected for further docking studies. The interactions between Piscisoflavone C and residues in 4BFO were shown in Fig. 5a, b. The binding energy formed was −8.3 kcal/mol, which was higher compared to the energy recorded by the Isomaltotriose interaction (Table 1). As presented in Fig. 4a, b, this phytochemical made two hydrogen bonds with amino acid residues Asn29 and Lys34. Furthermore, the Piscisoflavone C exhibited three hydrophobic interactions with Tyr32 and Phe58 *via* π-π stacked interaction and Pro61involved in alkyl interaction. It also established π-anion with Glu68.

As illustrated in Table 2, Piscisoflavone C is eligible for further studies based on Lipinski filter i.e. drug-likeness and has 55 % of predictive bioavailability with a synthetic accessibility score of 3.83. This compound is predicted for moderately soluble with a high gastrointestinal (GI) absorption rate, permeable to BBB (Blood-brain barrier) and a non-effluxable compound as it is non-substrate to P-glycoprotein (Pgp,) but might be not readily metabolized by Cytochrome P450 (CYP) class enzymes due to the inhibitory activity predicted for CYP2D6 and predictively can take a longer time to be excreted from the system. Compound 8-o-methylaverufin is eligible for further studies based on Lipinski filter i.e. drug-likeness with 55 % of predictive bioavailability score, synthetic accessibility score of 4.85. 8-*o*-methylaverufin is predicted for moderately soluble with a high GI absorption rate, non-permeable to BBB (Blood-brain barrier) and can be effluxed out as it is predicted to be a substrate for Pgp. Moreover, the prediction as an inhibitor to CYP1A2 and CYP2C19 may affect the metabolizing rate and process of metabolism and excretion. Meanwhile, Punicalagin is eligible for further studies based on the Lipinski filter i.e., drug-likeness with 55 % of predictive bioavailability with a synthetic accessibility score of 3.76. This compound is moderately soluble with a high GI absorption rate, non-permeable to BBB (Blood-brain barrier) and non-effluxable compound as it is non-substrate to Pgp, but might not be readily metabolized by CYP class enzymes and predictively can take a longer time to be excreted due to its predictive inhibitory properties to CYP2C19 and CYP2D6 enzymes. However, Hopeanolin violates the Lipinski filter i.e., drug-likeness with a higher molecular weight of more than 500 kDa. Compounds Vaticanol E, alpha-Viniferin and Pauciflorol A violate the Lipinski filter with a molecular weight of more than 500 kDa and more than 5 hydrogen bond donors. Compounds Vaticanol B, Dioscin and Punicalin all violate the Lipinski filter with a molecular weight of more than 500-kilodaltons, more than 5 hydrogen bond donors and more than 10 hydrogen bond acceptors. Hopeanolin, Vaticanol E, Vaticanol B, alpha-Viniferin, Pauciflorol A, Dioscin and Punicalin have a poor predictive bioavailability score ranging between 11 % and 17 % with high synthetic accessibility scores ranging from 6.24 to 10.0. Furthermore, Hopeanolin, Vaticanol E, alpha-Viniferin and Pauciflorol

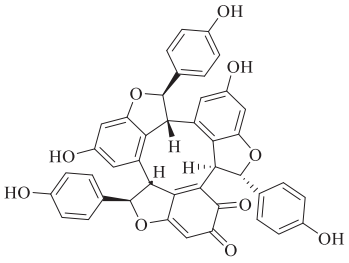

1

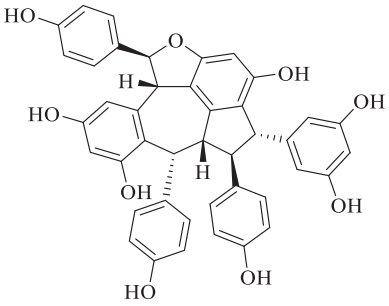

8

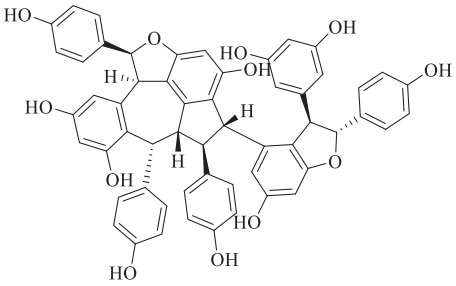

11

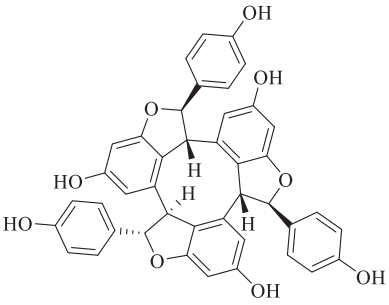

12

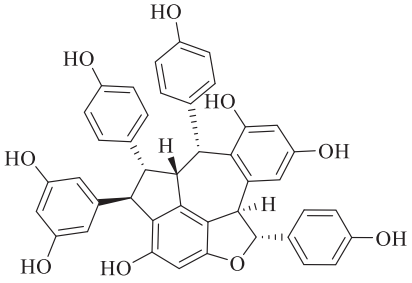

13

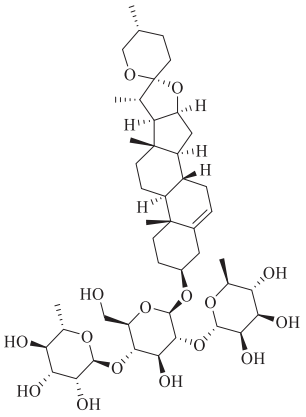

31

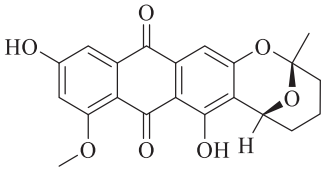

114

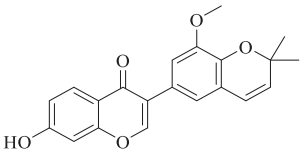

118

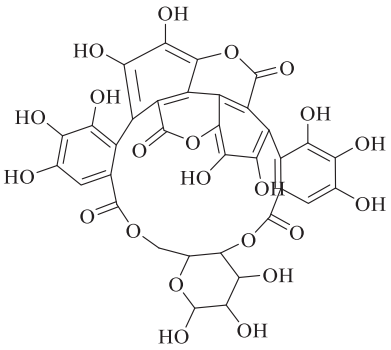

139

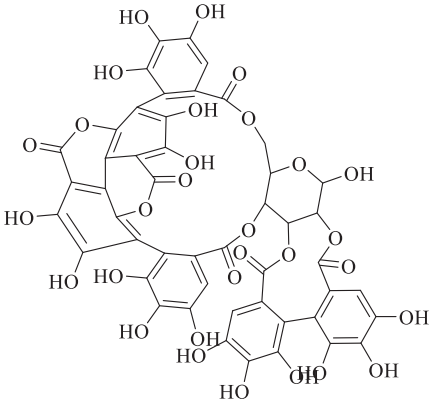

145

Fig. 3. Flowchart of the research work.

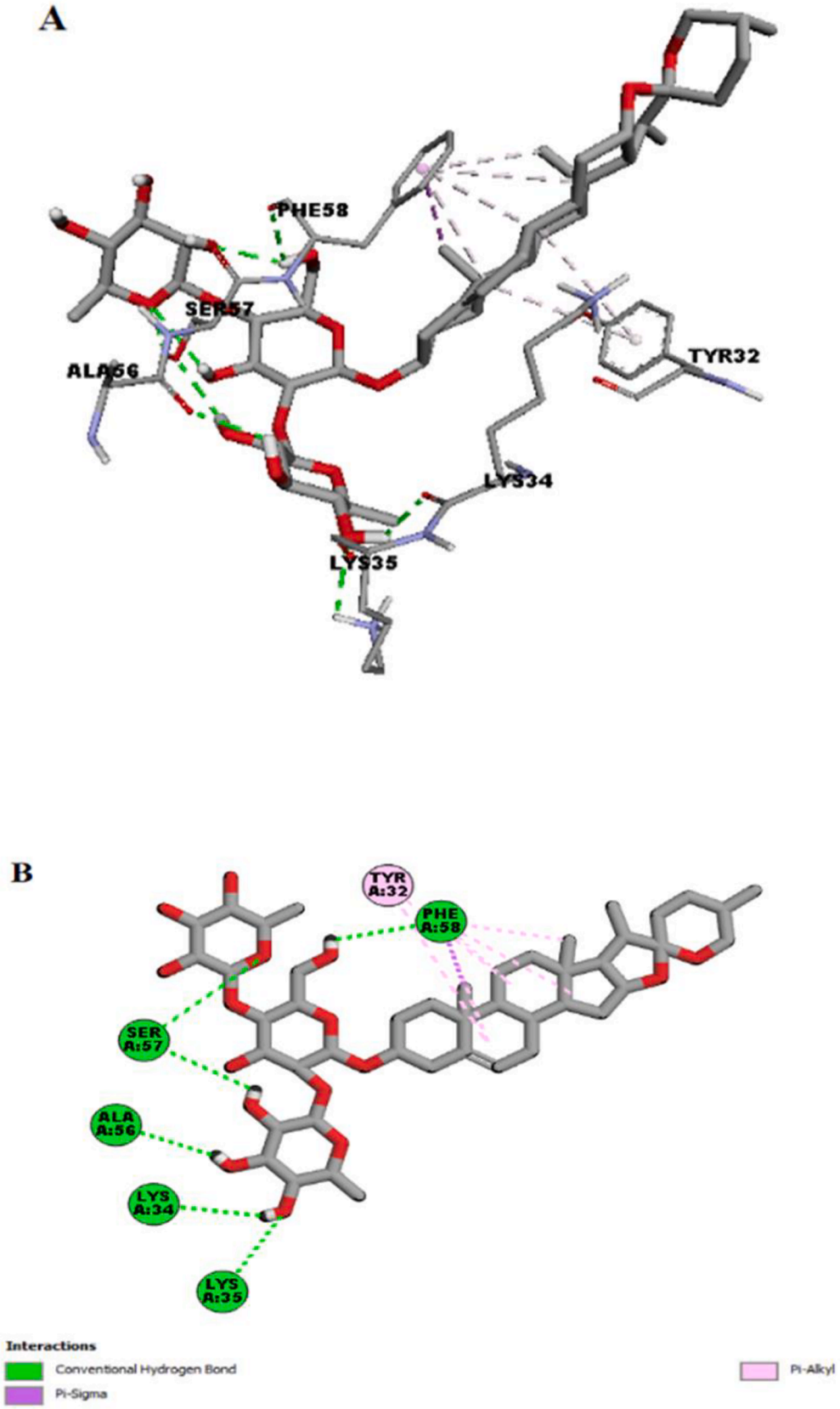

Fig. 4. The putative binding site of Dioscin on target protein (PDB ID: 4BFO). (**A**) Three-dimensional representation of important interactions. (**B**) 2D schematic diagram showing amino acids residues involved in interactions.

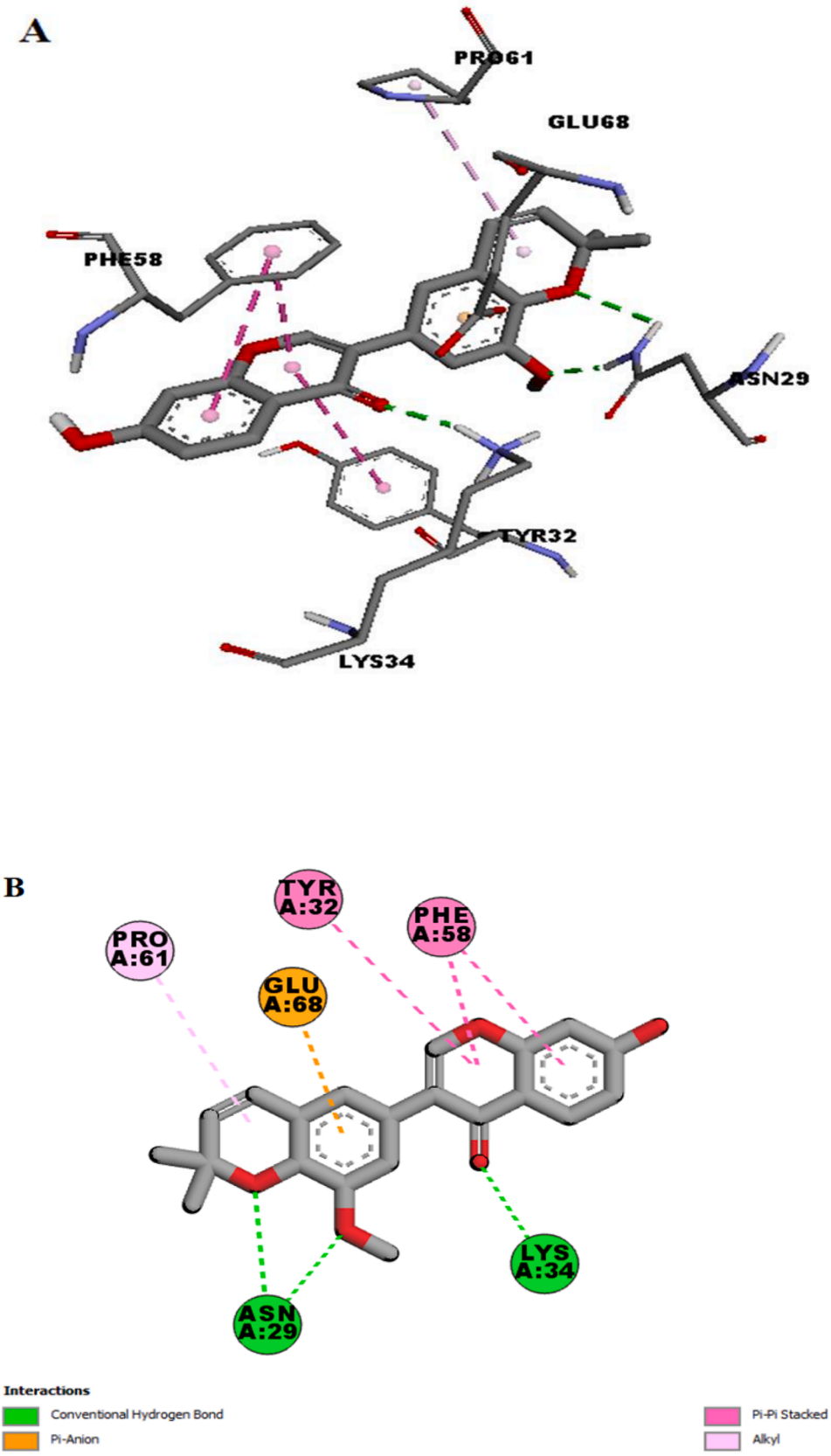

Fig. 5. The putative binding site of Piscisoflavone C on target protein (PDB ID: 4BFO). (**A**) Three-dimensional representation of important interactions. (**B**) 2D schematic diagram showing amino acids residues involved in interactions.

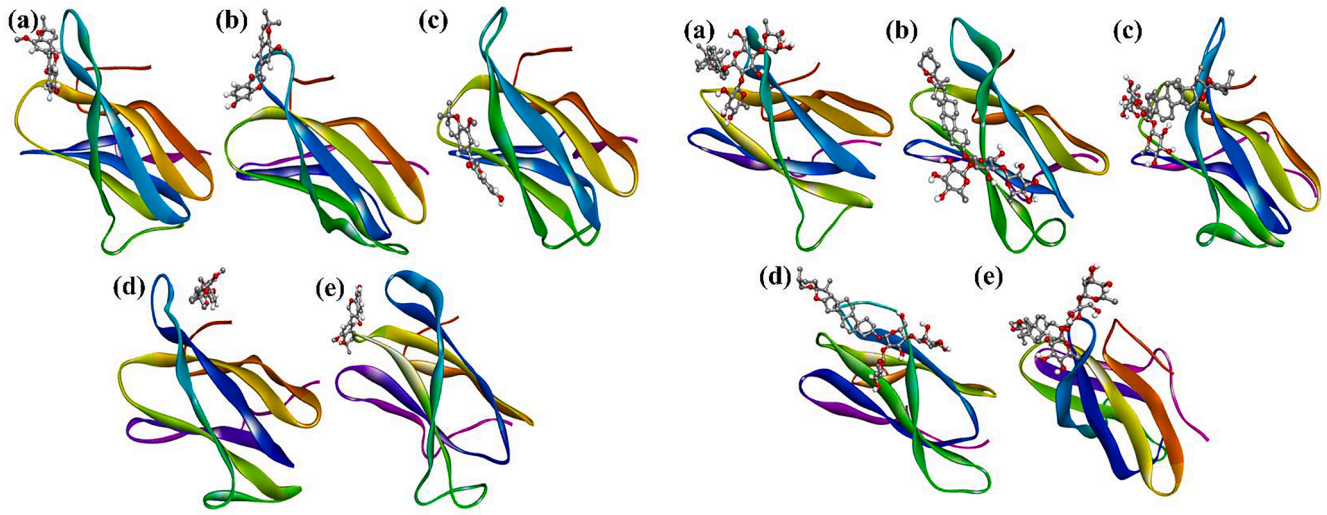

Fig. 6. (a). Protein-ligand structure of Dioscin at **(a)**1 ns, **(b)** 10 ns, **(c)** 20 ns, **(d)** 50 ns and **(e)** 100 ns MD run, giving a visual impression of the sequence of events and the dynamics of the process. Fig. 6 **(b).** Protein-ligand structure of Piscisoflavone C at**(a)** 1 ns, **(b)** 10 ns, **(c)** 20 ns, **(d)** 50 ns and **(e)** 100 ns MD run, giving a visual impression of the sequence of events and the dynamics of the process.

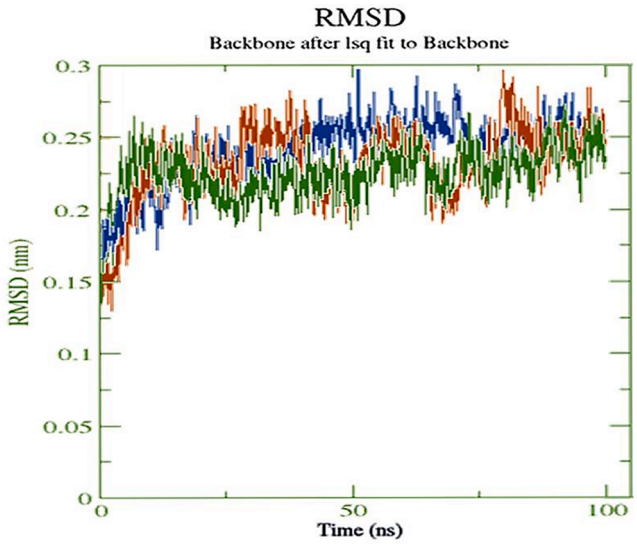

Fig. 7. The root mean square deviation (RMSD) plot of solvated protein backbone and ligand complex during 100 ns MD simulation for unbound protein (blue), Dioscin (brown color) and Piscisoflavone C (green color). (For interpretation of the references to color in this figure legend, the reader is referred to the web version of this article.)

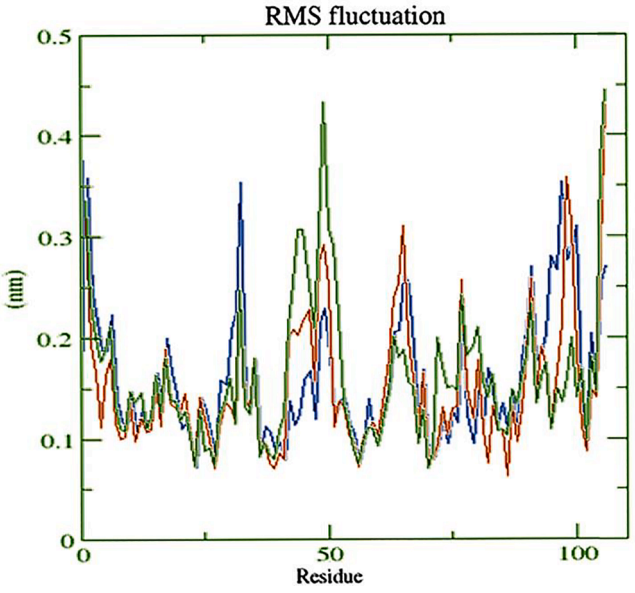

Fig. 8. The root mean square fluctuation (RMSF) plot of solvated unbound protein (blue), protein–ligand complex (Dioscin, brown color) and (Piscisoflavone C, green color) plotted against residue numbers. (For interpretation of the references to color in this figure legend, the reader is referred to the web version of this article.)

A predicted for a poor solubility, low GI absorption rate, non-permeable to BBB (Blood-brain barrier) and can be effluxed out as it is predicted as a substrate to Pgp, but might be readily metabolized by CYP class enzymes and predictively can easily be excreted through the system, because they fall under the prediction of the substrate to CYP class of enzyme. The compound Vaticanol B exhibited insolubility, low GI absorption rate, non-permeability to BBB (Blood-brain barrier), but it can be effluxed out as it is predicted to be a substrate to Pgp, but might be readily metabolized by CYP class enzymes and predictively can easily be excreted from the system, due to its prediction as a substrate to CYP class of enzyme. The Dioscin and Punicalin predicted for a moderately soluble, low GI absorption rate, non-permeable to BBB (Blood-brain barrier), the substrate to CYP class of enzyme hence might be readily metabolized and easily be excreted from the system. But and can be effluxed out as it is predicted as a substrate to Pgp.

The acute oral toxicity was calculated using admetSAR, following compounds exhibited a grade III oral acute toxicity (Table 3): Vaticanol E, Vaticanol B, alpha-Viniferin, Pauciflorol A, Dioscin, 8-o-methylaverufin, Piscisoflavone C, Punicalin and Punicalagin. Grade II oral toxicity was reported only for Hopeanolin. No compound was reported for Eye corrosion, whereas Piscisoflavone C and Punicalagin were reported for Eye irritation. Liver injury/hepatotoxicity was predicted and found only Dioscin to be safe with no hepatotoxicity. The inward rectifying voltage gated potassium channel in the heart (IKr), which is important in cardiac repolarization, is encoded by the human ether-a-go-go-related gene (hERG). Inhibition of the hERG current promotes the QT interval, resulting in Torsade de Pointes, a potentially fatal ventricular tachyarrhythmia. 8-o-methylaverufin, Piscisoflavone C and Punicalagin were predicted as non-inhibitor to hERG. On the other hand, AMES toxicity test was used to know whether a compound is mutagenic or not,

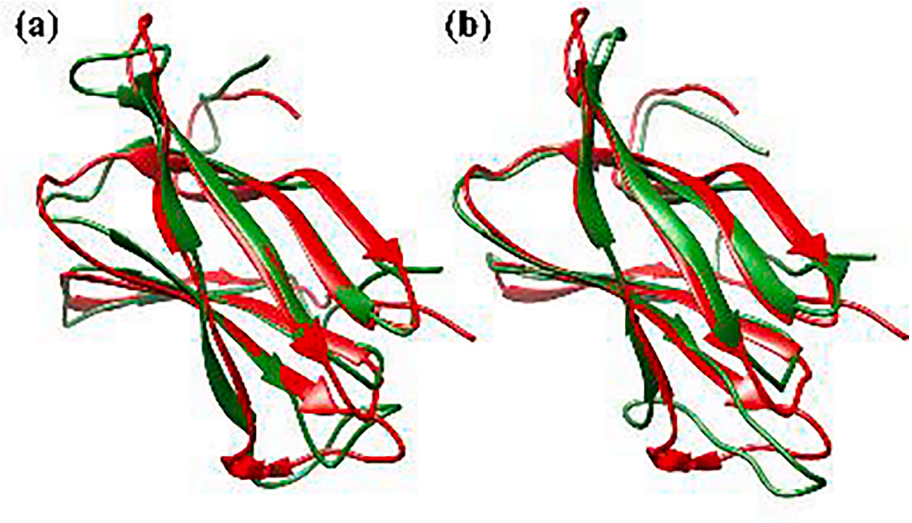

Fig. 9. Superimposed structure of unbounded protein (red) and protein after simulation (green)(**a**) Dioscin and (**b**) Piscisoflavone C. (For interpretation of the references to color in this figure legend, the reader is referred to the web version of this article.)

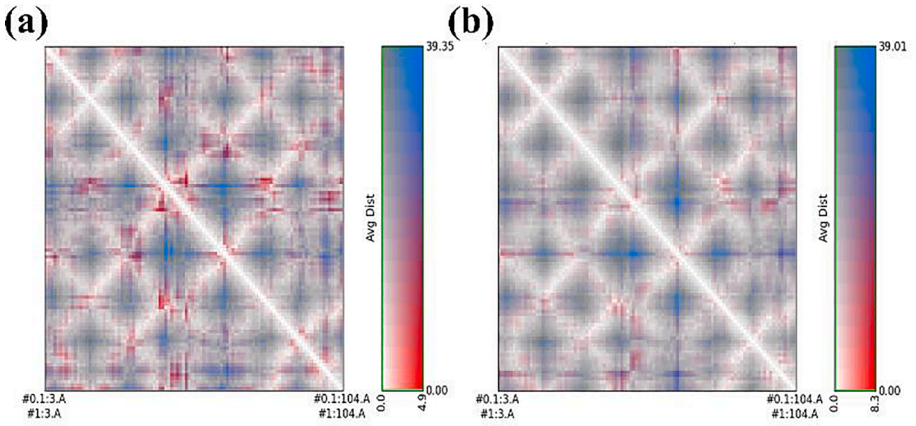

Fig. 10. RR distance map patterns of spatial interactions of the protein(**a**) Dioscin and (**b**) Piscisoflavone C showing the average distance and standard deviation for all amino acid pairs.

excluding Hopeanolin, 8-*o*-methylaverufin and Punicalin, all others are predicted as non-mutagenic in nature. As per carcinogenicity prediction, Hopeanolin, alpha-Viniferin and Piscisoflavone C gave positive signals for carcinogenesis, whereas others were marked safe. The micronuclear assay prediction reported a genotoxicity positive score for Hopeanolin, Vaticanol E, Vaticanol B, alpha-Viniferin, Pauciflorol A, Piscisoflavone C, Punicalin and Punicalagin. The compounds that were marked safe are Dioscin and 8-o-methylaverufin (Table 3).

The complexes simulations were showed no loss of structural integrity and compactness, which suggests good performance of the applied force field and adequate quality of the experimental structures were used as starting states for the simulations [137–139]. The conformational changes of the complex were studied during 1, 10, 20, 50 and 100 ns MD simulation run was depicted in Fig. 6 (a,b). The different structures represented in Fig. 6 (a,b) provide a visualization of the dynamics of the process and the sequence of events. Only the ligand is displayed as space-filling for better exhibition of the occurring motions, while the receptor is shown by its backbone. Molecular dynamics data are processed by calculating the RMSD (from the starting structure) to analyze structural stability. It is observed from Fig. 7 Piscisoflavone C complex exhibits the lowest RMSD than Dioscin complex. Even RMSD of the unbound-protein is slightly higher than the Piscisoflavone C, which indicates the greater stability of Piscisoflavone C. From the RMSD diagram the stable complex conformations of Dioscin and Piscisoflavone C were observed after ~ 60 and 85 ns, respectively, having RMSD values of ~ 2.8 and 2.2 Å, respectively (Fig. 7). According to the literature, RMSD value of less than 3.0 Å is the most acceptable, as the lower the RMSD value shows greater stability of complex [140,141]. The obtained results indicated that Piscisoflavone C forms a more stable protein–ligand complex than Dioscin and does not make any considerable conformational change in the protein structure during simulation study. The flexibility of each residue is computed to gain a better understanding of how the binding of a ligand changes the protein flexibility since RMSF aids in understanding the area of the protein that is being varied during the simulation. To assess the average fluctuation and flexibility of individual residues, the RMSF of protein and complexes were plotted using 100 ns MD trajectory, as shown in Fig. 8. The RMSF plot shows that the fluctuations of residues are occurring in the receptor at several times during the ligand-bound state and the binding makes the protein most flexible in all areas in contrast to unbound -protein and the other complex. The protein structure is found to have the lowest RMSF at some key residues, which indicates that even in unliganded state, the protein is not very much flexible. Overall, the residues are found flexible for both of unbound -protein and ligand-bound complexes. The lowest RMSF value of ~ 0.067 Å was found in the complex of Piscisoflavone C-receptor. The findings show that ligand–protein interaction brings protein chains

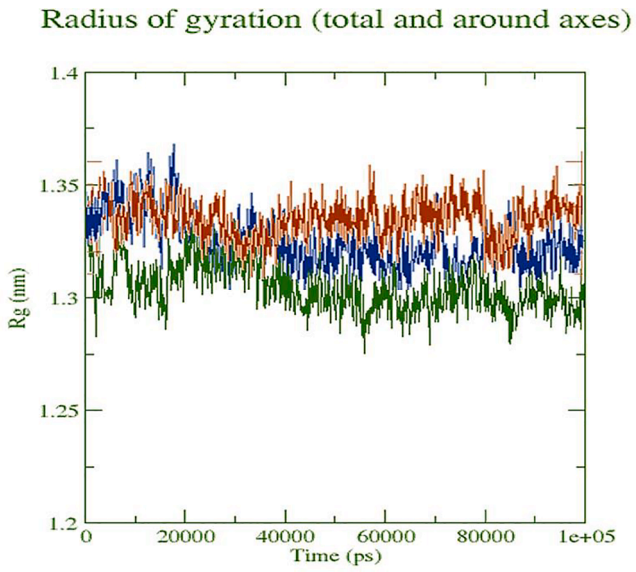

Fig. 11. Radius of gyration (Rg) of unbound protein (blue), protein–ligand complex (Dioscin, brown color) and (Piscisoflavone C, green color) during 100 ns simulation time. (For interpretation of the references to color in this figure legend, the reader is referred to the web version of this article.)

closer together and reduces the space between them, shown in Fig. 9. The standard deviation and average distance for all pairs of residue between two conformations are represented by RR (residue-residue) distance map (two-dimensional representations of protein 3D structure) and it was used for comparing and analyzing the structures of protein. The RR distance maps are represented in Fig. 10, which plots patterns of spatial interactions [142,143]. In the map, the white diagonal shows the zero distance between two residues, while the blue and red elements represent the residue pairings with the longest distance variances in the two conformations. A radius of gyration (Rg) plot was used to analyze the compactness of the ligand-bound protein. The lowest Rg value of ~ 12.75 Å was shown by Piscisoflavone C; on the other hand, Dioscin shows an Rg value of ~ 13.15 Å. Therefore, the order of compactness and rigidness should be Piscisoflavone C > unbound -protein > Dioscin. A decrease in Rg for complex along with the simulation time was found means an increase in the compactness of the structure (Fig. 11). A minute reduce in the Rg value of protein was observed upon interacting with Piscisoflavone C. As a result of the interacting of Piscisoflavone C, the microenvironment of receptor was altered, resulting in conformational changes in the structure of receptor.

As shown in Fig. 12, Grid-search on a 16x16x19 grid, rcut = 0.35, was used to calculate the hydrogen bond interactions established between ligand and protein, which was then plotted versus time. On calculating hydrogen bonds between ligands (32 atoms for Dioscin and 63 atoms for Piscisoflavone C) and protein (1100 atoms), 164donors and 303 acceptors were observed for Dioscin, whereas, 171 donors and 318 acceptors were observed for Piscisoflavone C. The average number of hydrogen bonds per timeframe was found to be 0.038 and 0.770out of 25,174 and 27,189 possible for Dioscin and Piscisoflavone C, respectively. Overall, it was observed that the ligand interaction with receptor dramatically enhanced the number of hydrogen bonds. During MD simulation in ligand-receptor bound conditions, the SASA of receptor was calculated. Interactions of the ligand-receptor leads to change of the SASA values (Fig. 13). The analysis displays the receptor folds and its stability when it binds to a ligand. The decrease of SASA vale of protein upon binding of ligand suggests that the structure of the receptor has altered, with a decreased pocket size and more hydrophobicity around it. The result of the MD simulation indicates the Piscisoflavone C complex is more stable and compact as compared to the Dioscin.

5. Conclusion

Mucormycosis is a rare opportunistic fungal infection, that attack individuals with weak immune system. Considering its high prevalence as post COVID-19 infection, the development of new antifungal agents, preferably with a novel mechanism of action, is an urgent medical need. In the present study, virtual screening of natural products was performed against the glucoamylase enzyme of Rhizopus oryzae through molecular docking. Docking studies revealed that most of the tested compounds showed good binding affinity with target enzyme. As per the *in-silico* predicted, ADMET analysis of compounds, Piscisoflavone C, 8-o-methylaverufin and Punicalagin exhibited positive outcomes considering no violation to Lipinski filter and drug-likeness properties and mild to moderate of toxicity. Molecular dynamics simulation of 100 ns run unveils that ligand Piscisoflavone C formed a more stable complex with receptor throughout the simulation time in comparison with Dioscin.

Declaration of Competing Interest

The authors declare that they have no known competing financial

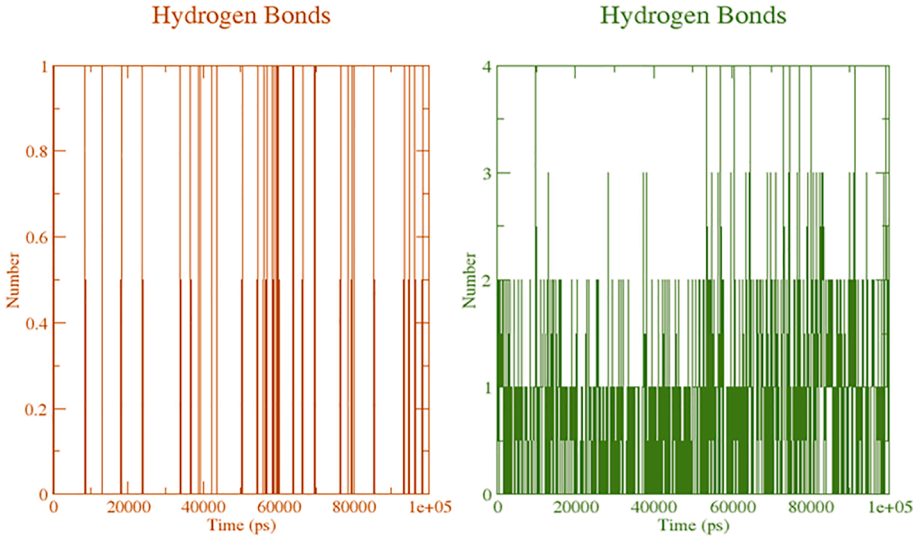

Fig. 12. Number of average hydrogen bonding interactions between protein–ligand complex (Dioscin, brown color) and (Piscisoflavone C, green color) during 100 ns simulation time. (For interpretation of the references to color in this figure legend, the reader is referred to the web version of this article.)

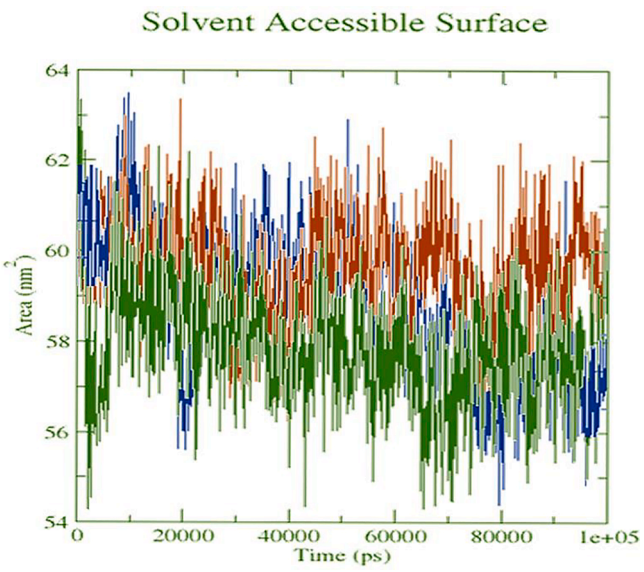

Fig. 13. Solvent accessible surface area (SASA) analysis for unbound protein (blue), protein–ligand complex (Dioscin, brown color and Piscisoflavone C, green color) during 100 ns simulation time. (For interpretation of the references to color in this figure legend, the reader is referred to the web version of this article.)

interests or personal relationships that could have appeared to influence the work reported in this paper.

Data availability

No data was used for the research described in the article.

Acknowledgments

NA.

References

[1] J.A. Ribes, C.L. Vanover-Sams, D.J. Baker, Zygomycetes in human disease, Clin. Microbiol. Rev. 13 (2) (2000) 236–301.
[2] M.L. Elgart, ZYGOMYCOSIS, Dermatol. Clin. 14 (1) (1996) 141–146.
[3] A. Paltauf, Mycosis mucorina, Archiv für pathologische Anatomie und Physiologie und für klinische Medicin 102 (3) (1885) 543–564.
[4] A.A. Elfiky, The antiviral Sofosbuvir against mucormycosis: an in silico perspective, Fut. Virol. 14 (11) (2019) 739–744.
[5] B. Spellberg, J. Edwards, A. Ibrahim, Novel Perspectives on Mucormycosis: Pathophysiology, Presentation, and Management, Clin. Microbiol. Rev. 18 (3) (2005) 556–569.
[6] P.N. Malani, Mandell, Douglas, and Bennett's principles and practice of infectious diseases, JAMA 304 (18) (2010) 2067–2071.
[7] M. Khan, et al., COVID-19: A Global Challenge with Old History, Epidemiology and Progress So Far, Molecules 26 (1) (2021) 39.
[8] P. Yang, X. Wang, COVID-19: a new challenge for human beings, Cell. Mol. Immunol. 17 (5) (2020) 555–557.
[9] Y. Jin, et al., Virology, Epidemiology, Pathogenesis, and Control of COVID-19, Viruses 12 (4) (2020).
[10] N.H.A. Huseen, Docking study of naringin binding with COVID-19 main protease enzyme, Iraqi Journal of Pharmaceutical Sciences 29 (2) (2020) 231–238.
[11] S. Gokulshankar, B. Mohanty, COVID-19 and black fungus, Asian J. Med. Health Sci. 4 (1) (2021) 138.
[12] K.S. Ebrahimi, et al., In silico investigation on the inhibitory effect of fungal secondary metabolites on RNA dependent RNA polymerase of SARS-CoV-II: A docking and molecular dynamic simulation study, Comput. Biol. Med. 135 (2021), 104613.
[13] I. Mahalaxmi, et al., Mucormycosis: An opportunistic pathogen during COVID-19, Environ. Res. 201 (2021), 111643.
[14] J. Pemán, et al., Fungal co-infection in COVID-19 patients: Should we be concerned? Revista Iberoamericana de Micología 37 (2) (2020) 41–46.
[15] V. Gade, et al., Mucormycosis: Tsunami of Fungal Infection after Second Wave of COVID 19, Annals of the Romanian Society for Cell Biology 25 (6) (2021) 6383–6390.
[16] M. Nambiar, S.R. Varma, M. Damdoum, Post-Covid alliance-mucormycosis, a fatal sequel to the pandemic in India, Saudi Journal of Biological Sciences (2021).
[17] V. Rao, et al., Post-COVID Mucormycosis in India: A formidable challenge, Br. J. Oral Maxillofac. Surg. (2021).
[18] Ghosh, T. and S. Chatterjee, *Evaluation of the effect of deadly mucormycosis in post covid-19 patients.* Turkish Journal of Physiotherapy and Rehabilitation. **32**(2): p. 337-3742.
[19] K. Hoang, et al., A case of invasive pulmonary mucormycosis resulting from short courses of corticosteroids in a well-controlled diabetic patient, Medical Mycology Case Reports 29 (2020) 22–24.
[20] S. Lim, et al., COVID-19 and diabetes mellitus: from pathophysiology to clinical management, Nature Reviews Endocrinology 17 (1) (2021) 11–30.
[21] W.K. Balwan, Epidemiology of Mucormycosis in India: A Notifiable Disease, Saudi J. Pathol. Microbiol. 6 (6) (2021) 187–191.
[22] K. Kwon-Chung, Mucormycosis (Phycomycosis, Zygomycosis), Med. Mycol. (1992) 524–559.
[23] Cornely, O.A., et al., Global guideline for the diagnosis and management of mucormycosis: an initiative of the European Confederation of Medical Mycology in cooperation with the Mycoses Study Group Education and Research Consortium. The Lancet Infectious Diseases, 2019. **19**(12): p. e405-e421.
[24] J.P. Gangneux, et al., Invasive fungal diseases during COVID-19: We should be prepared, Journal de mycologie medicale 30 (2) (2020), 100971.
[25] M.M. Roden, et al., Epidemiology and Outcome of Zygomycosis: A Review of 929 Reported Cases, Clin. Infect. Dis. 41 (5) (2005) 634–653.
[26] H. Prakash, A. Chakrabarti, Global Epidemiology of Mucormycosis, J. Fungi 5 (1) (2019) 26.
[27] A. Werthman-Ehrenreich, Mucormycosis with orbital compartment syndrome in a patient with COVID-19, Am. J. Emerg. Med. 42 (2021) 264.e5–264.e8.
[28] M.C. Chibucos, et al., An integrated genomic and transcriptomic survey of mucormycosis-causing fungi, Nat. Commun. 7 (1) (2016) 12218.
[29] S.S. Rawlani, et al., Black Fungus Mucormycosis, Epidemiology, Etiopathogenesis, Clinical Diagnosis, Histopathology and its Management-A Review, Int. J. Med. Dental Res. 1 (2) (2021) 1–8.
[30] A. Patel, et al., A multicentre observational study on the epidemiology, risk factors, management and outcomes of mucormycosis in India, Clin. Microbiol. Infect. 26 (7) (2020) 944.e9–944.e15.
[31] S. Husain, et al., Opportunistic Mycelial Fungal Infections in Organ Transplant Recipients: Emerging Importance of Non-Aspergillus Mycelial Fungi, Clin. Infect. Dis. 37 (2) (2003) 221–229.
[32] K.A. Marr, et al., Epidemiology and Outcome of Mould Infections in Hematopoietic Stem Cell Transplant Recipients, Clin. Infect. Dis. 34 (7) (2002) 909–917.
[33] D.P. Kontoyiannis, et al., Zygomycosis in the 1990s in a Tertiary-Care Cancer Center, Clin. Infect. Dis. 30 (6) (2000) 851–856.
[34] P. Livio, et al., Mucormycosis in hematologic patients, Haematologica 89 (2) (2004) 207–214.
[35] A. Xhaard, et al., Mucormycosis after allogeneic haematopoietic stem cell transplantation: a French Multicentre Cohort Study (2003–2008), Clin. Microbiol. Infect. 18 (10) (2012) E396–E400.
[36] M. Girardot, C. Imbert, Natural sources as innovative solutions against fungal biofilms, Fungal Biofilms and related infections (2016) 105–125.
[37] G. Lopes, E. Pinto, L. Salgueiro, Natural Products: An Alternative to Conventional Therapy for Dermatophytosis? Mycopathologia 182 (1) (2017) 143–167.
[38] T. Arif, et al., Natural products–antifungal agents derived from plants, J. Asian Nat. Prod. Res. 11 (7) (2009) 621–638.
[39] R. Serpa, et al., In vitro antifungal activity of the flavonoid baicalein against Candida species, J. Med. Microbiol. 61 (12) (2012) 1704–1708.
[40] S. Johann, et al., Antifungal properties of plants used in Brazilian traditional medicine against clinically relevant fungal pathogens, Brazilian Journal of Microbiology 38 (4) (2007) 632–637.
[41] Z. Liu, et al., Effects of Photodynamic Inactivation on the Growth and Antifungal Susceptibility of Rhizopus oryzae, Mycopathologia 184 (2) (2019) 315–319.
[42] K.W. Martin, E. Ernst, Herbal medicines for treatment of fungal infections: a systematic review of controlled clinical trials, Mycoses 47 (3–4) (2004) 87–92.
[43] M. Fahad, et al., As Antimicrobial Agents: Synthesis, Structural Characterization and Molecular Docking study of Barbituric Acid Derivatives from Phenobarbital, Chemical Methodologies 6 (2022) 122–136.
[44] S. Hammami, et al., Saoussanabiloïde, a novel antifungal alkaloid from Echiochilon fruticosum Desf. growing in Tunisia, Nat. Prod. Res. 23 (16) (2009) 1466–1471.
[45] M. Hussain, F.B., et al., Structure Elucidation of the spiro-Polyketide Svalbardine B from the Arctic Fungal Endophyte Poaceicola sp. E1PB with Support from Extensive ESI-MSn Interpretation. J. Nat. Prod., 2020. **83**(12): p. 3493-3501.
[46] S. Vengurlekar, R. Sharma, P. Trivedi, Efficacy of some natural compounds as antifungal agents, Pharmacogn. Rev. 6 (12) (2012) 91–99.
[47] M.F. Jiménez-Reyes, et al., Natural compounds: A sustainable alternative to the phytopathogens control, J. Chil. Chem. Soc. 64 (2) (2019) 4459–4465.
[48] M.J. Abad, M. Ansuategui, P. Bermejo, Active antifungal substances from natural sources, Arkivoc 7 (11) (2007) 116–145.
[49] M. Krogh-Madsen, et al., Amphotericin B and Caspofungin Resistance in Candida glabrata Isolates Recovered from a Critically Ill Patient, Clin. Infect. Dis. 42 (7) (2006) 938–944.
[50] S. Raveendran, et al., Applications of Microbial Enzymes in Food Industry, Food technology and biotechnology 56 (1) (2018) 16–30.
[51] P. Kumar, T. Satyanarayana, Microbial glucoamylases: characteristics and applications, Crit. Rev. Biotechnol. 29 (3) (2009) 225–255.

[52] Cantarel, B.L., et al., *The Carbohydrate-Active EnZymes database (CAZy): an expert resource for Glycogenomics.* Nucleic Acids Res, 2009. **37**(Database issue): p. D233-D238.

[53] J.-Y. Tung, et al., Crystal structures of the starch-binding domain from Rhizopus oryzae glucoamylase reveal a polysaccharide-binding path, Biochem. J. 416 (1) (2008) 27–36.

[54] M. Formela-Luboińska, et al., The Role of Saccharides in the Mechanisms of Pathogenicity of Fusarium oxysporum f. sp. lupini in Yellow Lupine (Lupinus luteus L.), Int. J. Mol. Sci. 21 (19) (2020) 7258.

[55] P.M. Coutinho, P.J. Reilly, Glucoamylase structural, functional, and evolutionary relationships, Proteins 29 (3) (1997) 334–347.

[56] J.J. Kelly, D.H. Alpers, *Properties of human intestinal glucoamylase.* Biochimica et Biophysica Acta (BBA), - Enzymology 315 (1) (1973) 113–122.

[57] T. Riaz, et al., Enzyme inhibitory, Antifungal, Antibacterial and hemolytic potential of various fractions of Colebrookia oppositifolia, Pak J Pharm Sci 30 (1) (2017) 105–112.

[58] G. Meshram, S. Khamkar, G. Metangale, Antimicrobial screening of Garlic (Allium sativum) extracts and their effect on Glucoamylase activity in-vitro, J. Appl. Pharm. Sci. 02 (01) (2012) 106–108.

[59] A. Mukherjee, S. Sengupta, Characterization of nimbidiol as a potent intestinal disaccharidase and glucoamylase inhibitor present in Azadirachta indica (neem) useful for the treatment of diabetes, J. Enzyme Inhib. Med. Chem. 28 (5) (2013) 900–910.

[60] A. Alqarihi, et al., GRP78 and Integrins Play Different Roles in Host Cell Invasion during Mucormycosis, mBio 11 (3) (2020) e01087–e10120.

[61] C. Baldin, A.S. Ibrahim, Molecular mechanisms of mucormycosis—The bitter and the sweet, PLoS Pathog. 13 (8) (2017) e1006408.

[62] T. Gebremariam, et al., CotH3 mediates fungal invasion of host cells during mucormycosis, J Clin Invest 124 (1) (2014) 237–250.

[63] H. Prakash, et al., Connecting the Dots: Interplay of Pathogenic Mechanisms between COVID-19 Disease and Mucormycosis, J. Fungi 7 (8) (2021) 616.

[64] H.R. Gazi, et al., Secondary Metabolites as Well as Antioxidant and P-Glucosidase Inhibitory Potential of Hopea Scaphula ROXB, Turk J Pharm Sci 9 (3) (2012) 335–342.

[65] Vikram, P., et al., *A review of phytochemicals and antimicrobial potentials of mahogany.* 2014.

[66] N.A. Evensen, P.C. Braun, The effects of tea polyphenols on Candida albicans: inhibition of biofilm formation and proteasome inactivation, Can. J. Microbiol. 55 (9) (2009) 1033–1039.

[67] R. Tan, et al., Secoiridoids and antifungal aromatic acids from Gentiana algida, Phytochemistry 41 (1) (1996) 111–116.

[68] A. Thawabteh, et al., The Biological Activity of Natural Alkaloids against Herbivores, Cancerous Cells and Pathogens, Toxins 11 (11) (2019) 656.

[69] M. Moriyama, et al., Isoflavones from the root bark of Piscidia erythrina, Phytochemistry 31 (2) (1992) 683–687.

[70] J.R. Zgoda-Pols, et al., Antimicrobial Resveratrol Tetramers from the Stem Bark of Vatica oblongifolia ssp. oblongifolia, J. Nat. Prod. 65 (11) (2002) 1554–1559.

[71] H. Punetha, S. Singh, A. Gaur, Antifungal and antibacterial activities of crude withanolides extract from the roots of Withania somnifera(L.) Dunal (Ashwagandha), Environ. Conserv. J. 11 (1–2) (2010) 65–69.

[72] S.A.M. Abdelgaleil, et al., Antifungal limonoids from the fruits of Khaya senegalensis, Fitoterapia 75 (6) (2004) 566–572.

[73] EL-Hefny, M., et al., The Potential Antibacterial and Antifungal Activities of Wood Treated with Withania somnifera Fruit Extract, and the Phenolic, Caffeine, and Flavonoid Composition of the Extract According to HPLC. Processes, 2020. **8** (1): p. 113.

[74] P. Kharel, et al., Isolation, identification and antimicrobial activity of a Withanolide [WS-1] from the roots of Withania somnifera, Nepal Journal of Science and Technology 12 (2011) 179–186.

[75] R.I. Misico, et al., Withanolides and related steroids, Prog. Chem. Org. Nat. Prod. 94 (2011) 127–229.

[76] V. Treyvaud Amiguet, et al., Phytochemistry and Antifungal Properties of the Newly Discovered Tree Pleodendron costaricense, J. Nat. Prod. 69 (7) (2006) 1005–1009.

[77] K.A. El Sayed, D.T.A. Youssef, D. Marchetti, Bioactive Natural and Semisynthetic Latrunculins, J. Nat. Prod. 69 (2) (2006) 219–223.

[78] Y.-H. Shen, et al., ent-Labdane Diterpenoids from Andrographis paniculata, J. Nat. Prod. 69 (3) (2006) 319–322.

[79] D.G. Lee, et al., Antifungal activity of pinosylvin from Pinus densiflora on turfgrass fungal diseases, J. Appl. Biol. Chem. 60 (3) (2017) 213–218.

[80] C. Guerrero-Perilla, F.A. Bernal, E.D. Coy-Barrera, Molecular docking study of naturallyoccurring compounds as inhibitors of N-myristoyl transferase towards antifungal agents discovery, Revista Colombiana de Ciencias Químico-Farmacéuticas 44 (2) (2015) 162–178.

[81] C. de Moura Martins, et al., Antifungal and cytotoxicity activities and new proanthocyanidins isolated from the barks of Inga laurina (Sw.) Willd, Phytochem. Lett. 40 (2020) 109–120.

[82] Z.-J. Li, et al., Antifungal Activity of Ellagic Acid In Vitro and In Vivo, Phytother. Res. 29 (7) (2015) 1019–1025.

[83] E. Rogozhin, et al., Characterization of Hydroxyproline-Containing Hairpin-Like Antimicrobial Peptide EcAMP1-Hyp from Barnyard Grass (Echinochloa crusgalli L.) Seeds: Structural Identification and Comparative Analysis of Antifungal Activity, Int. J. Mol. Sci. 19 (11) (2018) 3449.

[84] N. Delattin, et al., Plant-Derived Decapeptide OSIP108 Interferes with Candida albicans Biofilm Formation without Affecting Cell Viability, Antimicrob. Agents Chemother. 58 (5) (2014) 2647–2656.

[85] W. Chang, et al., Retigeric Acid B Enhances the Efficacy of Azoles Combating the Virulence and Biofilm Formation of Candida albican, Biol. Pharm. Bull. 35 (10) (2012) 1794–1801.

[86] P.A.S. White, et al., Antioxidant Activity and Mechanisms of Action of Natural Compounds Isolated from Lichens: A Systematic Review, Molecules 19 (9) (2014) 14496–14527.

[87] V.S. Thibane, et al., Effect of Marine Polyunsaturated Fatty Acids on Biofilm Formation of Candida albicans and Candida dubliniensis, Mar. Drugs 8 (10) (2010) 2597–2604.

[88] I.R.G. Capoci, et al., Propolis Is an Efficient Fungicide and Inhibitor of Biofilm Production by Vaginal Candida albicans, Evid. Based Compl. Alternat. Med. 2015 (2015), 287693.

[89] C.-F. Xie, et al., Antifungal macrocyclic bis(bibenzyls) from the Chinese liverwort Ptagiochasm intermedlum L, Nat. Prod. Res. 24 (6) (2010) 515–520.

[90] M. Ivanov, et al., Flavones, Flavonols, and Glycosylated Derivatives—Impact on Candida albicans Growth and Virulence, Expression of CDR1 and ERG11, Cytotoxicity, Pharmaceuticals 14 (1) (2021) 27.

[91] F.M. Porsche, et al., Antifungal Activity of Saponins from the Fruit Pericarp of Sapindus mukorossi against Venturia inaequalis and Botrytis cinerea, Plant Dis. 102 (5) (2018) 991–1000.

[92] M. Hirasawa, K. Takada, Multiple effects of green tea catechin on the antifungal activity of antimycotics against Candida albicans, J. Antimicrob. Chemother. 53 (2) (2004) 225–229.

[93] J. Safaei-Ghomi, A.A. Ahd, Antimicrobial and antifungal properties of the essential oil and methanol extracts of Eucalyptus largiflorens and Eucalyptus intertexta, Pharmacognosy magazine 6 (23) (2010) 172–175.

[94] D.G. Yun, D.G. Lee, *Silymarin exerts antifungal effects via membrane-targeted mode of action by increasing permeability and inducing oxidative stress.* Biochimica et Biophysica Acta (BBA) -, Biomembranes 1859 (3) (2017) 467–474.

[95] I. Dias, et al., Antifungal activity of linalool in cases of Candida spp. isolated from individuals with oral candidiasis, Br. J. Biol. 78 (2017) 368–374.

[96] M.S. Al Aboody, S. Mickymaray, Anti-Fungal Efficacy and Mechanisms of Flavonoids, Antibiotics 9 (2) (2020) 45.

[97] O. Elansary, H., et al., Antiproliferative, Antimicrobial, and Antifungal Activities of Polyphenol Extracts from Ferocactus Species. Processes, 2020. **8**(2): p. 138.

[98] A. Fatima, et al., Antifungal activity of Glycyrrhiza glabra extracts and its active constituent glabridin, Phytother. Res. 23 (8) (2009) 1190–1193.

[99] T.P.T. Cushnie, A.J. Lamb, Antimicrobial activity of flavonoids, Int. J. Antimicrob. Agents 26 (5) (2005) 343–356.

[100] O.A. Binutu, K.E. Adesogan, J.I. Okogun, Antibacterial and antifungal compounds from Kigelia pinnata, Planta Med. 62 (04) (1996) 352–353.

[101] P. Liu, et al., Antifungal activity of liquiritin in Phytophthora capsici comprises not only membrane-damage-mediated autophagy, apoptosis, and Ca2+ reduction but also an induced defense responses in pepper, Ecotoxicol. Environ. Saf. 209 (2021), 111813.

[102] Pistelli, L., et al., *Antimicrobial Activity of Inga fendleriana Extracts and Isolated Flavonoids.* Natural Product Communications, 2009. **4**(12): p. 1934578X0900401214.

[103] N.C. Veitch, Isoflavonoids of the Leguminosae, Nat. Prod. Rep. 26 (6) (2009) 776–802.

[104] R.P. Maskey, I. Grün-Wollny, H. Laatsch, Isolation, structure elucidation and biological activity of 8-O-methylaverufin and 1,8-O-dimethylaverantin as new antifungal agents from Penicillium chrysogenum, J. Antibiotics 56 (5) (2003) 459–463.

[105] M. Masi, et al., Phytotoxic Activity of Metabolites Isolated from Rutstroemia sp.n., the Causal Agent of Bleach Blonde Syndrome on Cheatgrass (Bromus tectorum), Molecules 23 (7) (2018) 1734.

[106] S.A. Abdelgaleil, F. Hashinaga, M. Nakatani, Antifungal activity of limonoids from Khaya ivorensis, Pest Manag. Sci. 61 (2) (2005) 186–190.

[107] V. Paritala, et al., Phytochemicals and antimicrobial potentials of mahogany family, Revista Brasileira de Farmacognosia 25 (2015) 61–83.

[108] C. Montagner, et al., Antifungal Activity of Coumarins, Zeitschrift für Naturforschung C 63 (1–2) (2008) 21–28.

[109] P. Curir, et al., The plant antifungal isoflavone genistein is metabolized by Armillaria mellea Vahl to give non-fungitoxic products, Plant Biosystems - An International Journal Dealing with all Aspects of Plant Biology 140 (2) (2006) 156–162.

[110] S.S. Dahham, et al., Studies on antibacterial and antifungal activity of pomegranate (Punica granatum L.), Am. Eurasian J. Agric. Environ. Sci 9 (3) (2010) 273–281.

[111] H.-Y. Sohn, C.-S. Kwon, K.-H. Son, Fungicidal effect of prenylated flavonol, papyriflavonol A, isolated from Broussonetia papyrifera (L.) vent. against Candida albicans, J. Microbiol. Biotechnol. 20 (10) (2010) 1397–1402.

[112] H. Edziri, et al., Antibacterial, Antifungal and Cytotoxic Activities of Two Flavonoids from Retama raetam Flowers, Molecules 17 (6) (2012) 7284–7293.

[113] R.R. Kurdelas, et al., Antifungal Activity of Extracts and Prenylated Coumarins Isolated from Baccharis darwinii Hook & Arn. (Asteraceae), Molecules 15 (7) (2010) 4898–4907.

[114] M.D. Hanwell, et al., Avogadro: an advanced semantic chemical editor, visualization, and analysis platform, J. Cheminf. 4 (1) (2012) 17.

[115] N.M. O'Boyle, et al., Open Babel: An open chemical toolbox, J. Cheminf. 3 (1) (2011) 33.

[116] S. Dallakyan, PyRx-python prescription v. 0.8, The Scripps Research Institute (2008. 2010.).

[117] C.-H. Chu, et al., Crystal structures of starch binding domain from Rhizopus oryzae glucoamylase in complex with isomaltooligosaccharide: Insights into

polysaccharide binding mechanism of CBM21 family, Proteins Struct. Funct. Bioinf. 82 (6) (2014) 1079–1085.
[118] G.M. Morris, et al., Automated docking using a Lamarckian genetic algorithm and an empirical binding free energy function, J. Comput. Chem. 19 (14) (1998) 1639–1662.
[119] O. Trott, A.J. Olson, AutoDock Vina: improving the speed and accuracy of docking with a new scoring function, efficient optimization, and multithreading, J. Comput. Chem. 31 (2) (2010) 455–461.
[120] A. Daina, O. Michielin, V. Zoete, SwissADME: a free web tool to evaluate pharmacokinetics, drug-likeness and medicinal chemistry friendliness of small molecules, Sci. Rep. 7 (1) (2017) 42717.
[121] H. Yang, et al., admetSAR 2.0: web-service for prediction and optimization of chemical ADMET properties, Bioinformatics 35 (6) (2018) 1067–1069.
[122] A.H. Hasan, et al., Novel thiophene Chalcones-Coumarin as acetylcholinesterase inhibitors: Design, synthesis, biological evaluation, molecular docking, ADMET prediction and molecular dynamics simulation, Bioorg. Chem. 119 (2022), 105572.
[123] K. Vanommeslaeghe, et al., CHARMM general force field: A force field for drug-like molecules compatible with the CHARMM all-atom additive biological force fields, J. Comput. Chem. 31 (4) (2010) 671–690.
[124] W. Yu, et al., Extension of the CHARMM General Force Field to sulfonyl-containing compounds and its utility in biomolecular simulations, J. Comput. Chem. 33 (31) (2012) 2451–2468.
[125] W.L. Jorgensen, et al., Comparison of simple potential functions for simulating liquid water, J. Chem. Phys. 79 (2) (1983) 926–935.
[126] Allen, M.P. and D.J. Tildesley, *Computer simulation of liquids*. 2017: Oxford university press.
[127] U. Essmann, et al., A smooth particle mesh Ewald method, J. Chem. Phys. 103 (19) (1995) 8577–8593.
[128] P.J. Steinbach, B.R. Brooks, New spherical-cutoff methods for long-range forces in macromolecular simulation, J. Comput. Chem. 15 (7) (1994) 667–683.
[129] W. Humphrey, A. Dalke, K. Schulten, VMD: Visual molecular dynamics, J. Mol. Graph. 14 (1) (1996) 33–38.
[130] DeLano, W.L. and S. Bromberg, *PyMOL user's guide*. DeLano Scientific LLC, 2004. **629**.
[131] A. Scalbert, Antimicrobial properties of tannins, Phytochemistry 30 (12) (1991) 3875–3883.
[132] L. Mendoza, M. Wilkens, A. Urzúa, Antimicrobial study of the resinous exudates and of diterpenoids and flavonoids isolated from some Chilean Pseudognaphalium (Asteraceae), J. Ethnopharmacol. 58 (2) (1997) 85–88.
[133] A. Angioni, et al., Chemical Composition, Seasonal Variability, and Antifungal Activity of Lavandula stoechas L. ssp. stoechas Essential Oils from Stem/Leaves and Flowers, J. Agric. Food. Chem. 54 (12) (2006) 4364–4370.
[134] S. Renault, et al., CAY-1, a novel antifungal compound from cayenne pepper, Med. Mycol. 41 (1) (2003) 75–81.
[135] A.J. de Lucca, et al., CAY-1, a fungicidal saponin from Capsicum sp. fruit, Med. Mycol. 40 (2) (2002) 131–137.
[136] S. Ferheen, et al., Haloxylines A and B, Antifungal and Cholinesterase Inhibiting Piperidine Alkaloids from Haloxylon salicornicum, Chem. Pharm. Bull. 53 (5) (2005) 570–572.
[137] J. Šponer, et al., RNA Structural Dynamics As Captured by Molecular Simulations: A Comprehensive Overview, Chem. Rev. 118 (8) (2018) 4177–4338.
[138] T.M. Link, P. Valentin-Hansen, R.G. Brennan, SStructure of Escherichia coli Hfq bound to polyriboadenylate RNA, Proc. Natl. Acad. Sci. 106 (46) (2009) 19292.
[139] X.Y. Pei, et al., Architectural principles for Hfq/Crc-mediated regulation of gene expression, eLife 8 (2019) e43158.
[140] I. Kufareva, R. Abagyan, Methods of protein structure comparison, in: Homology Modeling, Springer, 2011, pp. 231–257.
[141] A.H. Hasan, et al., In silico discovery of multi-targeting inhibitors for the COVID-19 treatment by molecular docking, molecular dynamics simulation studies, and ADMET predictions, Struct. Chem. (2022).
[142] S. Wu, Y. Zhang, A comprehensive assessment of sequence-based and template-based methods for protein contact prediction, Bioinformatics 24 (7) (2008) 924–931.
[143] M.D. Khan, et al., Low concentrated phosphorus sorption in aqueous medium on aragonite synthesized by carbonation of seashells: Optimization, kinetics, and mechanism study, J. Environ. Manage. 280 (2021), 111652.